THE JOURNAL OF GENE MEDICINE
J Gene Med 2005; **7**: 739–748.
Published online 31 January 2005 in Wiley InterScience (www.interscience.wiley.com). **DOI:** 10.1002/jgm.717

RESEARCH ARTICLE

New multivalent cationic lipids reveal bell curve for transfection efficiency versus membrane charge density: lipid–DNA complexes for gene delivery

Ayesha Ahmad[1]
Heather M. Evans[1]
Kai Ewert[1]
Cyril X. George[2]
Charles E. Samuel[2]
Cyrus R. Safinya[1]*

[1]*Departments of Materials, Physics, and Molecular, Cellular and Development Biology, University of California, Santa Barbara, Santa Barbara, CA 93106-5121, USA*

[2]*Molecular, Cellular and Developmental Biology Department, Biomolecular Science and Engineering Program, University of California, Santa Barbara, Santa Barbara, CA 93106, USA*

*Correspondence to:
Cyrus R. Safinya, Materials Research Laboratory, UC Santa Barbara, Santa Barbara, CA 93106, USA.
E-mail: safinya@mrl.ucsb.edu

Received: 22 July 2004
Revised: 9 September 2004
Accepted: 20 September 2004

Abstract

Background Gene carriers based on lipids or polymers – rather than on engineered viruses – constitute the latest technique for delivering genes into cells for gene therapy. Cationic liposome–DNA (CL-DNA) complexes have emerged as leading nonviral vectors in worldwide gene therapy clinical trials. To arrive at therapeutic dosages, however, their efficiency requires substantial further improvement.

Methods Newly synthesized multivalent lipids (MVLs) enable control of headgroup charge and size. Complexes comprised of MVLs and DNA have been characterized by X-ray diffraction and ethidium bromide displacement assays. Their transfection efficiency (TE) in L-cells was measured with a luciferase assay.

Results Plots of TE versus the membrane charge density (σ_M, average charge/unit area of membrane) for the MVLs and monovalent 2,3-dioleyloxypropyltrimethylammonium chloride (DOTAP) merge onto a universal, bell-shaped curve. This bell curve leads to the identification of three distinct regimes, related to interactions between complexes and cells: at low σ_M, TE increases with increasing σ_M; at intermediate σ_M, TE exhibits saturated behavior; and unexpectedly, at high σ_M, TE decreases with increasing σ_M.

Conclusions Complexes with low σ_M remain trapped in the endosome. In the high σ_M regime, accessible for the first time with the new MVLs, complexes escape by overcoming a kinetic barrier to fusion with the endosomal membrane (activated fusion), yet they exhibit a reduced level of efficiency, presumably due to the inability of the DNA to dissociate from the highly charged membranes in the cytosol. The intermediate, optimal regime reflects a compromise between the opposing demands on σ_M for endosomal escape and dissociation in the cytosol. Copyright © 2005 John Wiley & Sons, Ltd.

Keywords gene therapy; cationic lipids; transfection efficiency; membrane charge density

Introduction

Cationic liposome–DNA (CL-DNA) complexes are attracting considerable attention as gene vectors due to their safety and other inherent advantages over viral delivery methods [1,2]. These advantages

include ease and variability of preparation, lack of immunogenicity, and a capacity for DNA of unlimited size, allowing for delivery of human artificial chromosomes [3]. Recent setbacks in clinical trials with viral vectors, in particular a fatality induced by a severe inflammatory response [4] and insertional mutagenesis caused by retroviral vectors [5], have further promoted a diligent effort in developing efficient nonviral methods.

Currently, lipofection is a prevalent nonviral gene transfer technology used in clinical trials worldwide [6]. CLs for transfection typically consist of a mixture of cationic and neutral (helper) lipid. Numerous lipids with varied chemical and physical properties have been synthesized [7–9] to improve the transfection efficiencies of CL-DNA complexes to the level of viral vectors. These include multivalent lipids, which have been described as superior to their monovalent counterparts [10,11].

Despite this abundance of different cationic lipids, unifying themes and a comprehensive understanding of the interactions between CL-DNA complexes and mammalian cells are lacking. In order to rationally design and improve lipid-based delivery systems, however, such an understanding is essential. In particular, it is necessary to identify the interactions between the CL-DNA complexes and the cells along the transfection pathway to overcome the biological impediments to optimal transfection by directed alteration and optimization of CL-DNA complex formulations.

In part, the lack of mechanistic understanding of gene delivery by CL-DNA complexes is due to the large number of parameters involved. Few investigations to date include a complete examination of lipid performance as a function of lipid-bilayer composition and lipid/DNA charge ratio (ρ_{chg}). Even in comparative studies [12], typically only one or two data points per lipid are evaluated, allowing the ideal lipid composition (the ratio of neutral to cationic lipid) or cationic lipid/DNA ratio to be overlooked [10,11].

In previous experiments with commercially available lipids, Lin *et al*. identified the membrane charge density, σ_M, as a universal parameter for transfection by lamellar CL-DNA complexes, but the scope of these investigations was limited by the lipids used [13]. The membrane charge density is the average charge per unit area of the membrane. It is controlled by the ratio of neutral to cationic lipid in the liposome formulation. On the other hand, the lipid/DNA charge ratio, ρ_{chg}, is the number of charges on the cationic lipid divided by the number of charges on the DNA. In our experiments, we keep both the amount of DNA and ρ_{chg} (and thus the number of charges contributed by the cationic lipid) constant. Thus, σ_M is varied solely by changing the amount of neutral lipid per transfection assay, "diluting" the cationic lipid in the membrane.

The work reported here presents both a confirmation and a significant extension of the earlier findings. We have synthesized a set of new multivalent lipids (MVLs) through methodical variation of headgroup size and charge and have examined the dependence of transfection efficiency (TE) on two key parameters, lipid composition and lipid/DNA charge ratio, ρ_{chg}. The MVLs [14], which form lamellar DNA complexes alone and when mixed with neutral 1,2-dioleoyl-*sn*-glycero-3-phosphatidylcholine (DOPC), enabled us to systematically probe very high membrane charge densities for the first time. For all DNA complexes of the MVLs as well as monovalent 2,3-dioleyloxypropyltrimethylammonium chloride (DOTAP), TE plotted versus σ_M fits the same, bell-shaped curve, confirming σ_M as a universal parameter. The curve shows three distinct regimes of TE and a clear maximum of TE at an optimal charge density, $\sigma_M{}^*$. Here, the TE rivals that of hexagonal CL-DNA complexes. The optimal $\sigma_M{}^*$ of the universal curve shifts systematically with ρ_{chg}, with an increase in ρ_{chg} resulting in higher values for $\sigma_M{}^*$. Only the new, highly charged lipids investigated here have permitted unambiguous identification of the universal maximum in TE and its shift with ρ_{chg}, as well as the discovery of a third regime of TE, where TE decreases (not saturates) with increasing σ_M.

Materials and methods

Materials

The multivalent lipids (MVLs), MVL2 (molecular weight (MW) = 884.2 g/mol), MVL3 (MW = 977.8 g/mol), MVL5 (MW = 1552.7 g/mol), and TMVL5 (MW = 1253.0 g/mol) (Table 1), were synthesized according to the procedure previously described [14]. N_α,N_δ-Bis(Boc)-ornithine and N_δ-Boc-ornithine (Novabiochem) were used as the starting materials for MVL2 and MVL3, respectively. 2,2′-(Ethylenedioxy)diethylamine for TMVL5 was purchased from Aldrich. For all lipids except MVL2, the final deprotection was performed by dissolving of the protected lipid in trifluoroacetic acid (Fisher), incubating at room temperature for 30 min and drying in vacuum, in deviation from the published protocol [14]. As described below, cationic liposomes were prepared containing these lipids as well as the cationic lipid 2,3-dioleyloxypropyltrimethylammonium chloride (DOTAP, MW = 698.55 g/mol), in combination with the neutral lipids DOPC (MW = 786.13 g/mol) and 1,2-dioleoyl-*sn*-glycero-3-phosphatidylethanolamine (DOPE, MW = 744.05 g/mol), all from Avanti Polar Lipids. CL-DNA complexes were formed from these cationic liposomes and the appropriate DNA. For X-ray samples, ethidium bromide (EtBr) experiments, and transfection assays, highly purified λ-phage DNA (New England Biolabs), highly polymerized calf thymus DNA (Amersham Life Sciences) and pGL3 plasmid DNA containing the luciferase gene (Promega Corp.) were used, respectively.

Liposomes

Lipid mixtures were prepared volumetrically by combining chloroform/methanol (4 : 1) solutions of cationic and

Table 1.

Name (*max. chg.*)	Structure
MVL2 (+2)	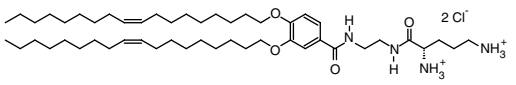
MVL3 (+3)	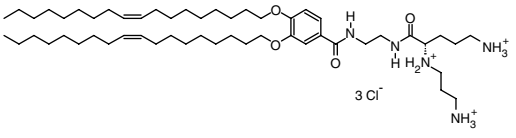
MVL5 (+5)	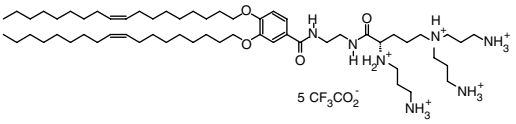
TMVL5 (+5)	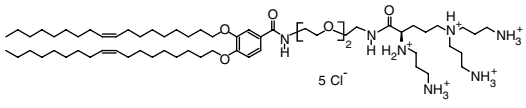

neutral lipids. The solvents were evaporated, first under a stream of nitrogen and subsequently in a high vacuum to ensure complete removal of the solvents. The dried lipid mixtures were hydrated at 37 °C for at least 6 h with the appropriate amount of deionized water of 18.2 MΩ (final concentration of 20 mg/ml for X-ray samples; final concentration of 0.5 mg/ml for transfection, and EtBr assay samples), sonicated to clarity with a VibraCell from Sonics and Materials Inc., and filtered through a 0.2 μm Teflon filter (Whatman). The obtained liposome solutions were stored at 4 °C.

Cell Transfection

Mouse fibroblast L-cells were cultured in Dulbecco's modified Eagle's medium (DMEM, Gibco BRL) supplemented with 1% (v/v) penicillin-streptomycin (Gibco BRL) and 5% (v/v) fetal bovine serum (Gibco BRL) at 37 °C in a humidified atmosphere with 5% CO_2, reseeding the cells every 2–4 days to maintain subconfluency. The cells were transfected at 60–80% confluency in 24-well plates (7 mm diameter per well). Liposome (0.5 mg/ml) and DNA (1 mg/ml) stock solutions were diluted with DMEM to a final volume of 0.1 ml and complexes, containing 0.4 μg of pGL3-DNA per well, were prepared at the desired cationic-to-anionic charge ratio (ρ_{chg}). The cells were incubated with the complexes for 6 h, rinsed three times with phosphate-buffered saline (PBS, Gibco BRL), and incubated in supplemented DMEM for an additional 24 h (sufficient for a complete cell cycle) to allow expression of the luciferase gene. Luciferase gene expression was measured with the luciferase assay system from Promega Corp., and light output readings were performed on a Berthold AutoLumat luminometer. Transfection efficiency, measured as relative light units (RLU), was normalized to the weight of total cellular protein using the Bio-Rad protein assay dye reagent. For experiments with chloroquine, complexes were formed in the same manner as above, but, prior to transfer to cells, the complexes were mixed with 1.8 μl of a 6 mg/ml chloroquine solution and incubated for 10 min. The normal transfection protocol was then resumed. To compensate for the variation in cell behavior over time, the data for DOTAP/DOPC complexes was normalized using data taken at the same time as TE data for MVL5.

X-ray diffraction (XRD)

CL-DNA complexes were prepared by mixing 75 μg of λ-phage DNA at 5 mg/ml with liposome solutions (20 mg/ml) in an Eppendorf centrifuge for approximately 3 h. Samples were prepared at $\rho_{chg} = 2.8$. After storage for 3 days at 4 °C, allowing the samples to reach equilibrium, they were transferred to 1.5 mm diameter quartz X-ray capillaries (Hilgenberg, Germany). The high-resolution XRD experiments were carried out at the Stanford Synchrotron Radiation Laboratory. Two-dimensional powder diffraction images were obtained using an image plate detector (Mar Instruments).

EtBr displacement assay

Samples were prepared in a 96-well plate. Each well contained 2.4 μg of DNA, 0.28 μg of EtBr and the appropriate amount of cationic lipid. Water was added to each well, achieving a final volume of 200 μl per well. Fluorescence was measured on a Cary Eclipse fluorescence spectrophotometer.

Results and discussion

MVL design and structures

Table 1 shows the chemical structures and maximum charges of the MVLs used in this study. These lipids were designed to achieve a systematic variation of the headgroup charge with minimal change in the chemical structure. Only a single aminopropyl unit per cationic charge was added to the headgroup, starting from the ornithine unit of MVL2. The oleyl chains provide strong anchoring in the membrane and miscibility with DOPC. TMVL5 has a slightly longer (triethylene glycol) spacer than the other MVLs.

X-ray characterization of MVL-DNA complexes shows a lamellar phase

We used XRD to determine the structure of MVL-DNA complexes. For all MVLs, at all investigated cationic/neutral lipid compositions of 0–90% DOPC, MVL-DNA complexes form the lamellar ($L_\alpha{}^C$) phase, the highly prevalent of the two known complex structures [15–17]. Moreover, XRD shows no evidence of phase separation, indicating that the complexes contain both

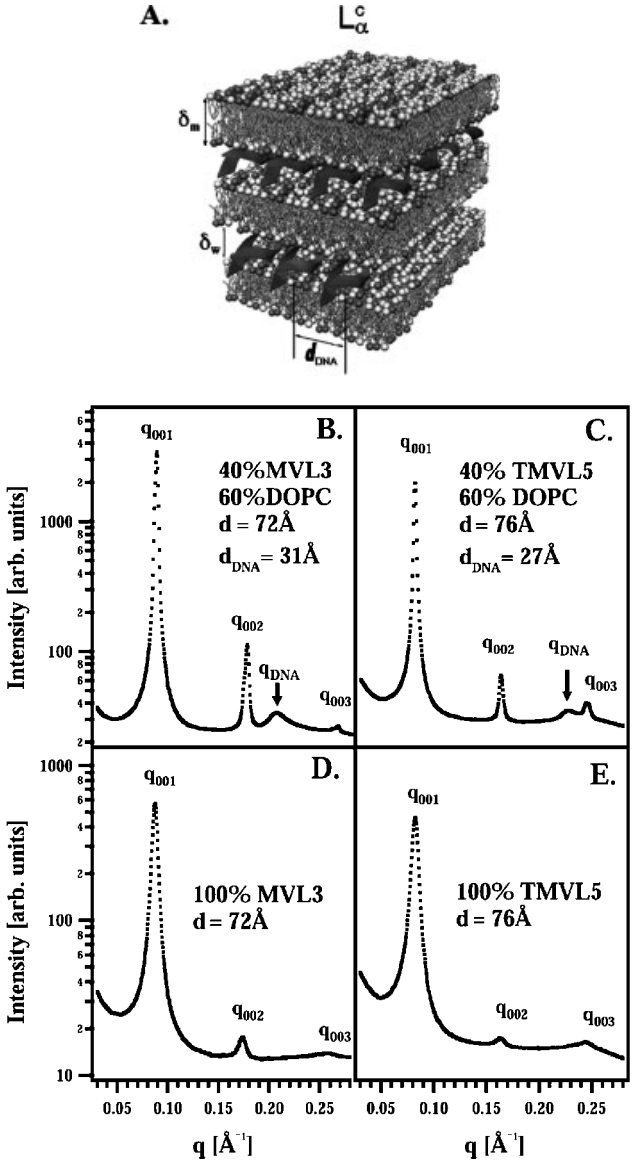

Figure 1. (A) Schematic of the lamellar phase indicating the characteristic dimensions. Reprinted with permission from [15]. (B, C) Typical X-ray diffraction (XRD) scans from lamellar ($L_\alpha{}^C$) CL-DNA complexes, containing 40 mol% MVL ((B) MVL3; (C) TMVL5) and 60 mol% DOPC, at a lipid/DNA charge ratio $\rho_{chg} = 2.8$ in the presence of DMEM. (D, E) Typical XRD scans from $L_\alpha{}^C$ CL-DNA complexes containing 100 mol% MVL ((D) MVL3; (E) TMVL5), prepared at $\rho_{chg} = 2.8$ in the presence of DMEM (Reproduced in part with permission from reference 15)

MVL and DOPC, as intended. A schematic of the lamellar phase ($L_\alpha{}^C$) and its characteristic dimensions is shown in Figure 1A. Figures 1B and 1C shows typical XRD patterns of complexes containing 40 mol% MVL (MVL3 (B); TMVL5 (C)) and 60 mol% DOPC, at a lipid/DNA charge ratio of 2.8, prepared in the presence of DMEM. The sharp peaks, labelled q_{001}, q_{002}, q_{003}, respectively, give the lamellar repeat distance, d, which is the sum of the membrane thickness (δ_m) and the thickness of a water/DNA layer (δ_w): $d = \delta_m + \delta_w = 2\pi/q_{001}$. The diffuse weaker peak, labeled q_{DNA}, results from one-dimensional ordering of the DNA sandwiched between the lipid bilayers and corresponds to a DNA interhelical spacing $d_{DNA} = 2\pi/q_{DNA}$ [17]. The experimental values are $d_{DNA} = 31$ Å for MVL3 and $d_{DNA} = 27$ Å for TMVL5. In Figures 1D and 1E, XRD patterns of complexes containing 100% MVL3 (D) and TMVL5 (E) under otherwise identical conditions are shown. The narrow peaks and multiple harmonics show that at the salt concentrations present in DMEM, i.e. under conditions as in the transfection experiments, stable and well-defined complexes form even from membranes containing exclusively the highly charged multivalent lipids. The salt present in DMEM screens the electrostatic repulsions between the headgroups and enables formation of stable complexes. However, when prepared in deionized water, complexes without neutral lipids exhibit broadening of the first lamellar peak (at q_{001}) and do not show higher harmonics of the first lamellar peak, indicative of smaller size multilamellar assemblies (results not shown).

Estimation of lipid headgroup charge: EtBr displacement assay

Figure 2 shows data from an EtBr displacement assay [18–21], performed to examine the ability of the MVLs to condense DNA within the CL-DNA complexes. The data was acquired by collecting fluorescence measurements at various weight ratios of MVL to DNA (with a fixed weight of DNA and EtBr per point) and normalizing the intensity to the fluorescence of DNA and EtBr in solution. EtBr fluoresces when intercalated between the base pairs of DNA, but self-quenches in solution. As the MVL liposomes are introduced and self-assembly into the $L_\alpha{}^C$ phase occurs, EtBr is displaced and overall fluorescence decreases until all DNA has been incorporated into the MVL-DNA complexes at the isoelectric point. Thus, this method allows a quick and efficient assessment of the effective charge on the headgroup of these lipids. The

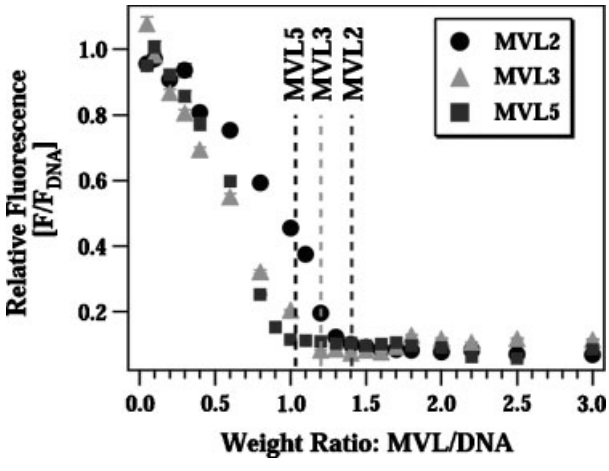

Figure 2. Normalized fluorescence data from the EtBr displacement assay for MVL2, MVL3 and MVL5. The dashed lines are drawn at the isoelectric points, determined as described in the text. They result in valencies of $Z_{MVL2} = 2.0 \pm 0.1$, $Z_{MVL3} = 2.5 \pm 0.1$, $Z_{MVL5} = Z_{TMVL5} = 4.5 \pm 0.1$

isoelectric point was determined as the intersection point of linear fits to the data at high and low lipid/DNA ratio [22,23]. This gives headgroup charges of $Z_{MVL2} = 2.0 \pm 0.1$, $Z_{MVL3} = 2.5 \pm 0.1$, $Z_{MVL5} = 4.5 \pm 0.1$. The dashed lines in Figure 2 indicate the corresponding isoelectric MVL/DNA weight ratios.

Transfection efficiency as a function of lipid composition

Figure 3 shows TE results for complexes transfecting mouse fibroblast cells at various MVL/DOPC ratios. Also included is data for the monovalent lipid DOTAP mixed with DOPC, a well-investigated reference system which constituted the starting point of our studies [13]. The complexes were prepared at $\rho_{chg} = 2.8$, which Lin *et al*. have found to be the optimum charge ratio for DOTAP/DOPC complexes [24]. The amount of DNA and cationic lipid per sample was kept constant. Thus, only the amount of neutral lipid varies between data points. All MVL-DNA complexes form globular particles of around 0.2 μm diameter in water, as previously reported for DOTAP [25] and MVL5 [14]. In DMEM, these particles form much larger aggregates due to screening of their electrostatic repulsion by the high salt concentration, as we have shown for MVL5 by optical and epi-fluorescence microscopy [14]. Figure 3A shows the TE data as a function of the molar fraction of cationic lipid. For all cationic lipids, a maximum in TE as a function of lipid composition is observed: at 65 mol% for MVL2, 70 mol% for MVL3, 50 mol% for MVL5, 55 mol% for TMVL5, and 90 mol% for DOTAP. The optimal molar ratio results in a TE that is over two decades higher than that of the lowest transfecting complexes in these systems, and each data set fits a skewed bell-shaped curve.

Membrane charge density is a universal parameter: three regimes of transfection efficiency

Figure 3B shows the data from Figure 3A plotted versus the membrane charge density, σ_M. A notable simplification occurs and all the data points merge onto a single curve. This identifies σ_M as a universal parameter for transfection by lamellar CL-DNA complexes.

As mentioned above, σ_M is the average charge per unit area of the lipid membrane; therefore, the headgroup areas of the lipids, their charge, and the molar fractions of cationic and neutral lipid are the parameters required to calculate σ_M. We calculated σ_M as described by Lin *et al*. [13], with σ_M = total charge/total membrane area $= eZN_{cl}/(N_{cl}\ A_{cl} + N_{nl}\ A_{nl}) = [1 - \Phi_{nl}/(\Phi_{nl} + r\Phi_{cl})]\sigma_{cl}$, where N_{cl} and N_{nl} are the number of cationic lipids and neutral lipids in the complexes, respectively; $r = A_{cl}/A_{nl}$ is the ratio of the headgroup areas of the cationic and the neutral lipid; $\sigma_{cl} = eZ/A_{cl}$ is the charge density of the cationic lipid with valence Z; and Φ_{nl} and Φ_{cl} are the molar fractions of the neutral and cationic lipids, respectively. For our data, we used $A_{nl} = 72$ Å^2 [26,27], $r_{DOTAP} = 1$, $r_{MVL2} = 1.05 \pm 0.05$, $r_{MVL3} = 1.30 \pm 0.05$, $r_{MVL5} = 2.3 \pm 0.1$, $r_{TMVL5} = 2.5 \pm 0.1$, $Z_{DOTAP} = 1$, $Z_{MVL2} = 2.0 \pm 0.1$, $Z_{MVL3} = 2.5 \pm 0.1$, $Z_{MVL5} = Z_{TMVL5} = 4.5 \pm 0.1$. The values for Z were obtained by the EtBr displacement assay as described above. The values for r can be considered as fitting parameters, but they yield physically reasonable values that agree with chemical intuition. (The values of r were determined based on agreement with the Gaussian fit. For the monovalent lipid DOTAP, r was assumed to be equal to 1, consistent with previous findings [13].) It is interesting to note that the optimal TE for MVL3 is found at a larger molar fraction of cationic lipid than for MVL2 despite the fact that MVL3 has a higher headgroup charge. This can be attributed to the significantly larger headgroup size of MVL3 and shows the importance of the parameter r.

The resulting curve of TE vs. σ_M can be described empirically by a simple Gaussian (solid line in Figure 3B):

$$TE = TE_0 + A\ \exp -[(\sigma_M - \sigma_M{}^*)/w]^2 \qquad (1)$$

where $TE_0 = -(1.9 \pm 5.6) \times 10^7$ RLU/mg protein; $A = (9.4 \pm 0.6) \times 10^8$ RLU/mg protein; $w = (5.8 \pm 0.5) \times 10^{-3}$ e/Å^2. For the optimal charge density, the fit gives $\sigma_M{}^* = (17.4 \pm 0.2) \times 10^{-3}$ e/Å^2.

Remarkably, in extension of previous results which showed the increase and a subsequent levelling-off of TE with σ_M [13], we see an entire bell curve of efficiency, including a decrease in TE at higher charge densities. Previously, without the series of new MVLs, Lin *et al*. were not adequately prepared to measure this range of charge densities.

The new universal TE curve of lamellar complexes exhibits three well-defined regimes. Regime I (dark gray), corresponding to low σ_M, features an exponential increase in efficiency over three orders of magnitude. Regime III (light gray), corresponding to high σ_M, is characterized by a decrease in efficiency with increasing σ_M, suggesting that there also is an obstacle of electrostatic nature to successful DNA delivery by lamellar CL-DNA complexes. The competition of the two effects that give rise to regimes I and III leads to the existence of the intermediate regime II (white) as the region of optimal charge density, corresponding to the highest TE. This clearly demonstrates the importance of including neutral lipid in the formulation of CL-DNA complexes, particularly those of newer, multivalent lipids. Due to the universality of the curve, it should also be possible to estimate the optimal composition for any given lipid by performing the simple EtBr displacement assay and estimating the headgroup size of the lipid from its chemical structure. We will address the implications of the universal curve for the mechanism of transfection in more detail below.

In addition to data for the lamellar complexes, Figure 3B shows TE data for the commonly used DOTAP/DOPE lipid system. The inverted hexagonal ($H_{II}{}^C$)

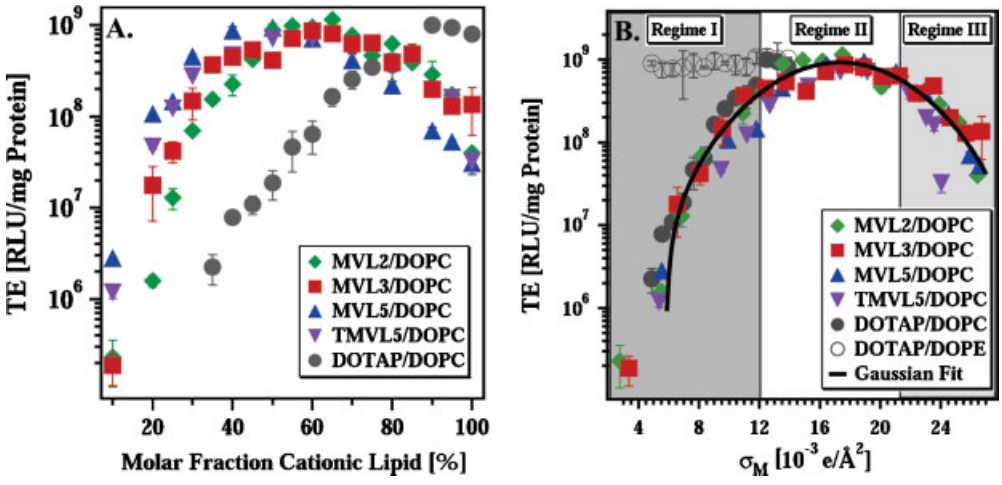

Figure 3. (A) TE in RLU per mg total cellular protein plotted as a function of mol% DOPC for DNA complexes prepared with MVL2 (green diamonds), MVL3 (red squares), MVL5 (blue triangles) and TMVL5 (purple inverted triangles) as well as DOTAP (gray circles). All data was taken at $\rho_{chg} = 2.8$, using the same amount of DNA for each data point. (B) The same TE data plotted against the membrane charge density, σ_M. Also included are data for DOTAP/DOPE complexes (gray open circles) and a Gaussian fit to the DOPC systems. The three regimes of transfection efficiency are indicated by different shading in the plot

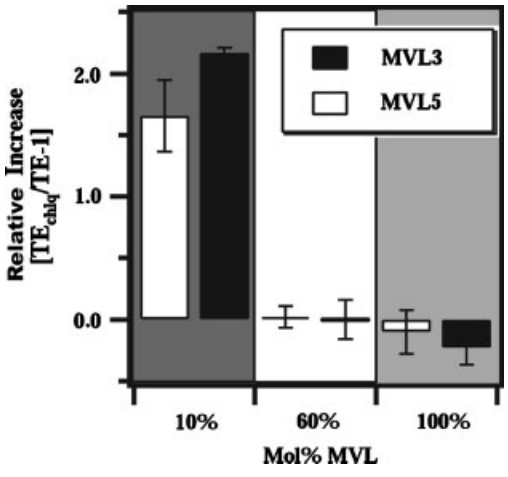

Figure 4. TE data taken in the presence of chloroquine (chlq) to assess the relevance of endosomal escape in the three regimes (regime I, dark gray; regime II, white; regime III, light gray). The relative increase in TE, $TE_{chlq}/TE\text{-}1$, is plotted for MVL3 (black bars) and MVL5 (white bars) in the three regimes. TE is enhanced by about a factor of three in regime I (10 mol% MVL), but not in regime II (60 mol% MVL) and regime III (100% MVL). This indicates that endosomal release is not a limiting factor for regimes II and III

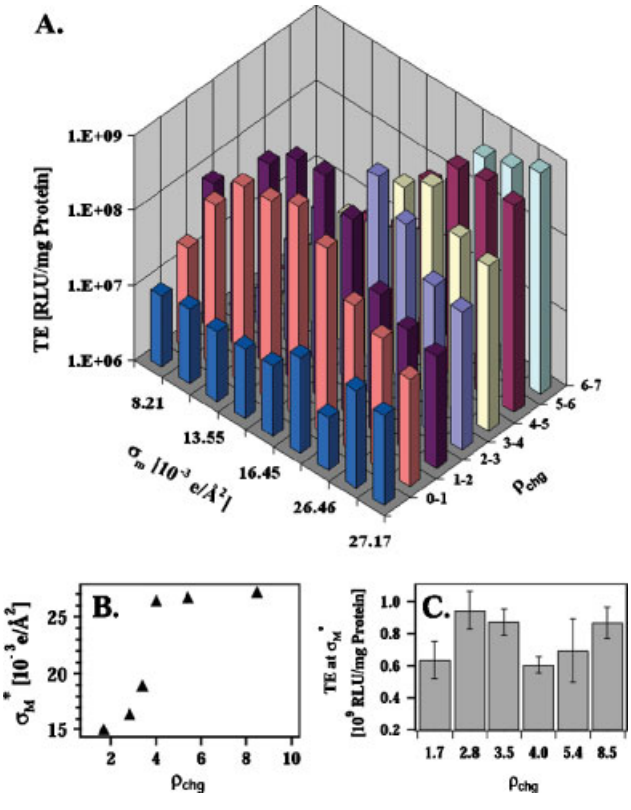

Figure 5. (A) Three-dimensional transfection phase diagram of lamellar complexes, combining data for MVL2, MVL3, and MVL5. Membrane charge density, σ_M, lipid/DNA charge ratio, ρ_{chg}, and TE are plotted along the x-axis, y-axis, and z-axis, respectively. (B) The optimal σ_M^* (from the data shown in (A)) is plotted against the charge ratio, ρ_{chg}. (C) The maximum TE (at σ_M^*) plotted against ρ_{chg}. This TE essentially remains constant

[15] DOTAP/DOPE complexes exhibit high TE even at low σ_M, due to their distinct mechanism of cellular entry, which relies on the fusogenic properties of DOPE [2,13]. This has made DOPE a popular choice as a co-lipid, and complexes with DOPE are abundant in the literature. However, the vast majority of neutral lipids lead to lamellar CL-DNA complexes, and, even with PE-based lipids, the hexagonal phase is only observed in a small window of composition [15]. Furthermore, the *in vivo* performance of PE-based complexes is disappointingly poor and cholesterol, which leads to lamellar complexes, is increasingly used as a neutral lipid for *in vivo* applications [2,7]. Therefore, our result that the TE of optimized $L_\alpha{}^C$ complexes rivals that of the highly transfecting $H_{II}{}^C$ DOTAP/DOPE complexes is of great significance. It adds a compositional degree of freedom, because efficiently transfecting complexes can be prepared from a broad

range of lipids without diminishing TE if σ_M is optimized. This includes lipids with specialized functions in the delivery process, such as peptide-lipids.

Effect of chloroquine on transfection efficiency in the three regimes

Endocytosis is the dominant mechanism of entry of lamellar CL-DNA complexes, as evident from recent confocal microscopy and transfection data [13] and work from other laboratories [28,29]. After cellular uptake via endocytosis, CL-DNA complexes must escape from endosomes in order for the DNA to progress toward the cell nucleus. Only a finite amount of time is available for this, since the endosomal pathway involves degradation of the contents of the endosome: initially through a lowering of the pH within the endosome and then through fusion with low-pH lysosomes.

The importance of endosomal escape as a barrier to transfection can be assessed by performing transfection experiments in the presence of chloroquine (chlq), a well-established bio-assay known to enhance the release of material from endosomes by osmotically bursting the vesicle [30]. We have repeated efficiency experiments for MVL3 and MVL5 in the presence of chloroquine for data points characteristic of the three transfection regimes. The resulting data is shown in Figure 4, plotted as the relative increase in transfection efficiency, $(TE_{chlq}\text{-}TE)/TE = TE_{chlq}/TE - 1$. TE in regimes II (60 mol% MVL) and III (100% MVL) is not enhanced by the addition of chloroquine. However, an increase in TE is seen in regime I, at low σ_M (10 mol% MVL), where transfection efficiency is enhanced approximately threefold. These results suggest that complexes with lower σ_M remain trapped within endosomes, while complexes with higher σ_M are able to overcome this barrier. Therefore, the decrease in TE at highest σ_M, in regime III, is not related to endosomal entrapment but must be due to other effects.

In regime I, a straight line fits the data of Figure 3B well, particularly for small values of σ_M. This regime was previously investigated by Lin *et al.* [13], who proposed that endosomal escape limits TE in this regime, consistent with the enhancement of TE by chloroquine. The escape from the endosome likely occurs via an activated fusion process of the oppositely charged membranes of endosome and complex [13]. The activation energy for this can be written as $\delta E = a\kappa - b\sigma_M$, where a and b are constants >0. The parameter κ is the bending rigidity of the membrane, which is mainly determined by the lipid tails and the area per lipid chain and therefore constant in our experiments. Bending of membranes, as required for fusion, results in an energy cost proportional to κ. Since the interacting membranes are oppositely charged, the activation energy decreases with increasing σ_M, making fusion with the endosomal membrane more likely. For endosomal entrapment being the main impediment to transfection as proposed by Lin *et al.*, the activation energy for fusion directly relates σ_M to the transfection efficiency via an Arrhenius-type equation [13]:

$$TE \propto \text{rate of fusion} = 1/\tau \; e^{-\delta E/kT} \qquad (2)$$

Here, $1/\tau$ is the collision rate between the trapped CL-DNA particle and the endosomal membrane.

At higher charge densities, in regimes II and III, TE is no longer limited by endosomal escape, as shown by the negligible effect of chloroquine. Here, the data of Figure 3B bends strongly away from a straight line but is well approximated by the empirical bell curve of Equation (1). Except for the lowest values of σ_M, this bell curve also fits the data in regime I, implying that the activation energy δE most likely contains contributions both linear and quadratic in σ_M.

Effect of lipid/DNA charge ratio: transfection phase diagram

All data shown in Figure 3 were taken at a fixed lipid/DNA charge ratio, ρ_{chg}, of 2.8. For other values of ρ_{chg}, we have observed similar, universal behavior. An efficiency phase diagram, shown in Figure 5A, summarizes these results. In this graph, σ_M varies along the x-axis, ρ_{chg} along the y-axis, and TE along the z-axis. At very low lipid/DNA charge ratios (i.e. below and near the isoelectric point, $\rho_{chg} \leq 1$, where complexes are negatively charged or neutral), TE is low for all values of σ_M. This is to be expected, as an overall positive CL-DNA charge is required to promote initial electrostatic interactions with cell membranes [31–33]. As ρ_{chg} is increased to above unity, a maximum in TE, defining the optimal membrane charge density $\sigma_M{}^*$, emerges and a bell curve of efficiency is observed, with the optimal $\sigma_M{}^*$ shifting to higher values with increasing ρ_{chg}. This means that much more cationic lipid is required to achieve optimal TE at large lipid/DNA charge ratios. For clarity, this surprising trend is shown in Figure 5B, which plots the optimal $\sigma_M{}^*$ against ρ_{chg}. The descending part of the bell curve beyond the optimal $\sigma_M{}^*$ for $\rho_{chg} > 1$ (i.e. regime III) cannot be seen for the highest lipid/DNA charge ratios. However, it seems likely that, given liposomes with an even higher charge density than the 27.17×10^{-3} e/Å^2 attainable with 100% MVL5, the decrease in the efficiency predicted by the bell curve shape would also be seen for the highest ρ_{chg}. As shown in Figure 5C, the maximum TE (TE at the optimal $\sigma_M{}^*$) does not change appreciably with ρ_{chg}. A relatively low lipid/DNA charge ratio, therefore, can be considered optimal since it allows for achievement of maximum TE with the least amount of cationic lipid. This is due to the unexpected increase of $\sigma_M{}^*$ with ρ_{chg}. Minimizing the amount of cationic lipid is desirable to reduce cost as well as potential toxic effects of the cationic lipid. In addition, achieving a given σ_M with fewer, more highly charged molecules should mean a smaller metabolic effort for the elimination of the lipids from the cell. This reasoning would favor multivalent over monovalent lipids. In this

context, it is important to note that with the amounts of cationic lipid employed in our *in vitro* experiments, we find no toxic effects on the cells as judged by cell morphology and the amount of total cellular protein.

A model of the intracellular CL-DNA complex pathway as a function of σ_M

The schematic shown in Figure 6 summarizes our current understanding of the cellular fate of $L_\alpha{}^C$ complexes in the three regimes. Initial attachment mediated by electrostatic attractions between CL-DNA complexes and negative charges at the cell surface (Figure 6a) is followed by endocytosis of the complex particle (Figure 6b), resulting in endosomal entrapment (Figure 6c) [13,31,34]. If cellular attachment and uptake were limiting TE via a σ_M-dependent mechanism, a linear increase of TE with σ_M would be predicted. Thus, our data, which shows an exponential increase, excludes this possibility.

For complexes with low $\sigma_M < \sigma_M{}^*$ (regime I), transfection is limited by endosomal escape (Figure 6d), as modelled by Equation (2) [13]. This is substantiated by the transfection experiments performed in the presence of chloroquine. These experiments also indicate that complexes with high σ_M (in regimes II and III) are able to escape from endosomes, most likely by activated fusion of the membranes of the CL-DNA complex and the endosome (Figure 6e). The complexes are then released into the cytoplasm (Figures 6f and 6g). Therefore, the unexpected new behavior observed at very high $\sigma_M > \sigma_M{}^*$ (regime III), where TE decreases with σ_M, must be due to another efficiency limiting mechanism. In the cytoplasm, the onion-like lamellar complexes are expected to dissociate layer by layer, slowly releasing their DNA. This likely occurs through interactions with anionic proteins, such as the abundant cytoskeletal protein actin, which readily forms complexes with CLs [35]. We hypothesize that transfection in regime III is limited by a slowed CL-DNA complex dissociation in the cytoplasm (Figure 6f vs. Figure 6g) due to the electrostatic interactions between the lipid bilayers and the DNA becoming stronger with increasing σ_M [25]. Previous work by other groups has shown that lipids chemically designed to be cleaved in the cytoplasm lead to enhanced TE, possibly by promoting complex dissociation [36,37].

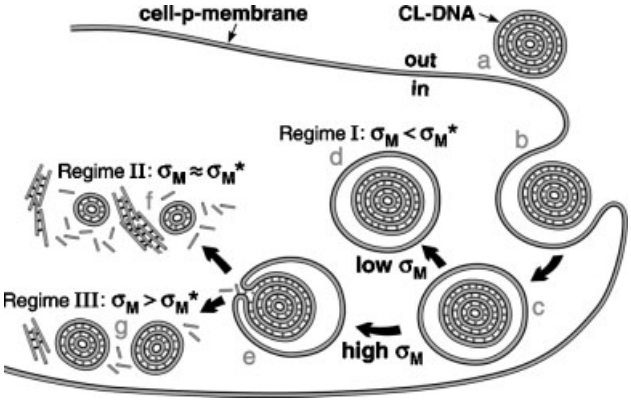

Figure 6. Model of cellular uptake of $L_\alpha{}^C$ complexes. Cationic complexes adhere to cells due to electrostatics (a) and enter through endocytosis (b and c). Low-σ_M complexes largely remain trapped in the endosome (d). High-σ_M complexes are able to escape the endosome through activated fusion (e). They release DNA through interactions with oppositely charged cellular biomolecules. We hypothesize that strong membrane–DNA interactions at very high charge density lead to diminished dissociation (g), while the complexes efficiently release their DNA at $\sigma_M \approx \sigma_M{}^*$ (f)

More work is required to confirm this hypothesis, and to check whether other effects, such as a dependence of κ on σ_M, play a role. Very fast escape from the endosome might also be unfavorable because it would prevent the complex from taking advantage of the trafficking of endosomes towards the nucleus.

In a recent theoretical paper, Hed and Safran [38] have considered the interactions between two oppositely charged membranes mimicking, for example, the interactions between cationic membranes of CL-DNA complexes and anionic membranes of the endosomes (Figures 6c, 6d, and 6e). Within mean field theory, two oppositely charged membranes of unequal σ_M repel each other due to counterion pressure. However, Hed and Safran predict that such asymmetrically charged membranes can exhibit regions of attractive interactions, due to charge density fluctuations. Such local interactions lead to fusion. Thus, the mechanism described by this model may be the origin of fusion and release of CL-DNA complexes from endosomes (Figure 6e).

Conclusions

We have established membrane charge density, σ_M, as a key universal parameter governing the transfection efficiency of CL-DNA complexes in the $L_\alpha{}^C$ phase. Using newly synthesized multivalent lipids, we were able to show that TE follows a universal, bell-shaped curve when plotted as a function of σ_M. The maximum of this universal curve shifts systematically with ρ_{chg}, with an increase in ρ_{chg} shifting the maximum TE to higher σ_M. At an optimal ρ_{chg}, we have identified three distinct regimes of TE, corresponding to low, intermediate and high σ_M. The maximum TE in regime II reflects the compromise between opposing requirements (Figure 6f): escape from endosomes requires high σ_M, but dissociation of complexes in the cytoplasm requires low σ_M. Future strategies for optimization must decouple these opposing requirements, e.g. by inclusion of a third component, which enhances TE in regimes I or III without affecting σ_M. One approach would be to modify other parameters affecting the energy barrier to endosomal fusion, such as the membrane bending rigidity. Another approach could involve introducing specific interactions via derivatives of PEG-lipids. By themselves, PEG-lipids of sufficient chain length are able to block the unspecific electrostatic interactions between cells and CL-DNA complexes [39].

The universality of the observed behavior in combination with identification and understanding of the three regimes is a powerful tool for predicting the composition range of optimal efficiency for any lipid system forming $L_\alpha{}^C$ complexes. Future work will investigate whether the universality can be extended to saturated lipid chains, for example, or systems where the initial cell adhesion is not charge-mediated. The detailed study presented here focuses on one particular cell line, but preliminary experiments show similar trends in other cell lines such as COS-1 and He-La. This is not surprising, as the initial interaction of CL-DNA complexes with cells is generally electrostatic in nature, relying on the positively charged complexes and the presence of negatively charged components on and in the cell plasma membrane. Of primary significance is the discovery that high TE can be achieved with lamellar complexes and at relatively low lipid/DNA charge ratios (where σ_M is an intermediate value). This ability to use fewer cationic molecules for high TE is important for cost reduction and possibly *in vivo* toxicity of cationic components. The presented transfection optimization strategy is directly relevant for gene therapy using *ex vivo* methods, where cells are removed, transfected, and returned to patients after selection. Further work on model systems relating to *in vivo* gene therapy is in progress.

Acknowledgements

We thank Blaine Butler for developing our ethidium bromide displacement protocol. Our work is supported by NIH GM-59288, AI-20611, and AI-12520. This work made use of MRL Central Facilities supported by the MRSEC Program of the National Science Foundation under award no. DMR00-80034.

References

1. For very recent reviews, see *Curr Med Chem* Vols. **10**(2003; issue 14) and **11** (2004, issue 2).
2. Mahato RI, Kim SW (eds). *Pharmaceutical Perspectives of Nucleic Acid Based Therapeutics*, Taylor and Francis: London, 2002.
3. Wilard HF. Genomics and gene therapy: artificial chromosomes coming to life. *Science* 2000; **290**: 1308–1309.
4. Raper SE, Chirmule N, Lee FS, *et al*. Fatal systemic inflammatory response syndrome in a ornithine transcarbamylase deficient patient following adenoviral gene transfer. *Mol Genet Metab* 2003; **80**: 148–158.
5. Hacein-Bey-Abina S, von Kalle C, Schmidt M, *et al*. A serious adverse event after successful gene therapy for X-linked severe combined immunodeficiency. *N Engl J Med* 2003; **348**: 255–256.
6. Edelstein ML, Abedi MR, Wixon J, Edelstein RM. Gene therapy clinical trials worldwide 1989–2004 – an overview. *J Gene Med* 2004; **6**: 597–602.
7. *Curr Med Chem* 2003; **10**: 1185–1315.
8. Miller AD. Cationic liposomes for gene delivery. *Angew Chem Int Ed Engl* 1998; **37**: 1768–1785.
9. Chesnoy S, Huang L. Structure and function of lipid-DNA complexes for gene delivery. *Annu Rev Biophys Biomol Struct* 2000; **29**: 27–47.
10. Byk G, Dubertret C, Escriou V, *et al*. Synthesis, activity, and structure-activity relationship studies of novel cationic lipids for DNA transfer. *J Med Chem* 1998; **41**: 224–235.
11. Remy JS, Sirlin C, Vierling P, *et al*. Gene transfer with a series of lipophilic DNA-binding molecules. *Bioconjugate Chem* 1994; **5**: 647–654.
12. Simberg D, Hirsch-Lerner D, Nissim R, *et al*. Comparison of different commercially available cationic lipid-based transfection kits. *J Liposome Res* 2000; **10**: 1–13.
13. Lin AJ, Slack NL, Ahmad A, *et al*. Three-dimensional imaging of lipid gene-carriers: membrane charge density controls universal transfection behavior in lamellar cationic liposome-DNA complexes. *Biophys J* 2003; **84**: 3307–3316.
14. Ewert K, Ahmad A, Evans HM, *et al*. Efficient synthesis and cell-transfection properties of a new multivalent cationic lipid for nonviral gene delivery. *J Med Chem* 2002; **45**: 5023–5029.
15. Koltover I, Salditt T, Rädler JO, *et al*. An inverted hexagonal phase of cationic liposome-DNA complexes related to DNA release and delivery. *Science* 1998; **281**: 78–81.
16. Lasic DD, Strey HH, Stuart MCA, *et al*. The structure of DNA-liposome complexes. *J Am Chem Soc* 1997; **119**: 832–833.
17. Rädler JO, Koltover I, Salditt T, *et al*. Structure of DNA-cationic liposome complexes: DNA intercalation in multilamellar membranes in distinct interhelical packing regimes. *Science* 1997; **275**: 810–814.
18. Xu Y, Szoka FC Jr. Mechanism of DNA release from cationic liposome/DNA complexes used in cell transfection. *Biochemistry* 1996; **35**: 5616–5623.
19. Even-Chen S, Barenholz Y. DOTAP cationic liposomes prefer relaxed over supercoiled plasmids. *Biochim Biophys Acta-Biomembr* 2000; **1509**: 176–188.
20. Eastman SJ, Siegel C, Tousignant J, *et al*. Biophysical characterization of cationic lipid : DNA complexes. *Biochim Biophys Acta-Biomembr* 1997; **1325**: 41–62.
21. Akao T, Fukumoto A, Ihara H, *et al*. Conformational change in DNA induced by cationic bilayer membranes. *FEBS Lett* 1996; **391**: 215–218.
22. Ham YW, Tse WC, Boger DL. High-resolution assessment of protein DNA binding affinity and selectivity utilizing a fluorescent intercalator displacement (FID) assay. *Bioorg Med Chem Lett* 2003; **13**: 3805–3807.
23. Boger DL, Fink BE, Brunette SR, *et al*. A simple, high-resolution method for establishing DNA binding affinity and sequence selectivity. *J Am Chem Soc* 2001; **123**: 5878–5891.
24. Lin AJ, Slack NL, Ahmad A, *et al*. Structure and structure-function studies of lipid/plasmid DNA complexes. *J Drug Target* 2000; **8**: 13–27.
25. Koltover I, Salditt T, Safinya CR. Phase diagram, stability, and overcharging of lamellar cationic lipid-DNA self-assembled complexes. *Biophys J* 1999; **77**: 915–924.
26. Tristram-Nagle S, Petrache HI, Nagle JF. Structure and interactions of fully hydrated dioleoylphosphatidylcholine bilayers. *Biophys J* 1998; **75**: 917–925.
27. Gruner SM, Tate MW, Kirk GL, *et al*. X-ray diffraction study of the polymorphic behavior of N-methylated dioleoylphosphatidylethanolamine. *Biochemistry* 1988; **27**: 2853–2866.
28. Mukherjee S, Ghosh RN, Maxfield FR. Endocytosis. *Physiol Rev* 1997; **77**: 759–803.
29. El Ouahabi A, Thiry M, Pector V, *et al*. The role of endosome destabilizing activity in the gene transfer process mediated by cationic lipids. *FEBS Lett* 1997; **414**: 187–192.
30. Felgner PL. Particulate systems and polymers for in vitro and in vivo delivery of polynucleotides. *Adv Drug Deliv Rev* 1990; **5**: 163–187.
31. Mislick KA, Baldeschwieler JD. Evidence for the role of proteoglycans in cation-mediated gene transfer. *Proc Natl Acad Sci U S A* 1996; **93**: 12 349–12 354.
32. Mounkes LC, Zhong W, Cipres-Palacin G, *et al*. Proteoglycans mediate cationic liposome-DNA complex-based gene delivery in vitro and in vivo. *J Biol Chem* 1998; **273**: 26 164–26 170.
33. Kopatz I, Remy JS, Behr JP. A model for non-viral gene delivery: through syndecan adhesion molecules and powered by actin. *J Gene Med* 2004; **6**: 769–776.
34. Zabner J, Fasbender AJ, Moninger T, *et al*. Cellular and molecular barriers to gene transfer by a cationic lipid. *J Biol Chem* 1995; **270**: 18 997–19 007.
35. Wong GCL, Tang JX, Lin A, *et al*. Hierarchical self-assembly of F-actin and cationic lipid complexes: stacked three-layer tubule networks. *Science* 2000; **288**: 2035–2039.
36. Byk G, Wetzer B, Frederic M, *et al*. Reduction-sensitive lipopolyamines as a novel nonviral gene delivery system for

modulated release of DNA with improved transgene expression. *J Med Chem* 2000; **43**: 4377–4387.
37. Tang F, Hughes JA. Use of dithiodiglycolic acid as a tether for cationic lipids decreases the cytotoxicity and increases transgene expression of plasmid DNA in vitro. *Bioconjugate Chem* 1999; **10**: 791–796.
38. Hed G, Safran SA. Attractive instability of oppositely charged membranes induced by charge density fluctuations. *Phys Rev Lett* 2004; **93**: 138101-1–138101-4.
39. Martin-Herranz A, Ahmad A, Evans HM, *et al*. Surface functionalized cationic lipid-DNA complexes for gene delivery: PEGylated lamellar complexes exhibit distinct DNA-DNA interaction regimes. *Biophys J* 2004; **86**: 1160–1168.